

Displacement of Yield Stress Fluids in Inclined Pipes

Kamran Alba¹, Seyed Mohammad Taghavi², Ian A. Frigaard^{1,2}

¹Department of Mechanical Engineering, University of British Columbia, Canada.

²Department of Mathematics, University of British Columbia, Canada

ABSTRACT

We present results of a primarily experimental study of buoyant miscible displacement flows of a yield stress fluid by a higher density Newtonian fluid along a long inclined pipe. We focus on the industrially interesting case where the yield stress is significantly larger than a typical viscous stress in the displacing fluid, but where buoyancy forces may be significant. We identify distinct flow regimes and observe exotic behaviours due to the large yield stress of the displaced fluid. We present the phenomenology of the flow regimes observed. We also find non-uniform static residual layers.

INTRODUCTION

There are many industrial processes in which it is necessary to remove a gelled material or soft-solid from a duct. Examples include bio-medical applications (mucus¹, biofilms²), cleaning of equipment and food processing³, oil well cementing⁴ and waxy crude oil pipeline restarts⁵. A wide range of material models are used to describe residual deposits in these situations. Some of these flows are turbulent, but equally often process limitations dictate that the flows be laminar. It is this case that we study here. Our industrial motivation comes from the oil industry, (both mud removal and waxy crude oil restarts), and we assume that the residual fluids in each case have a

yield stress. We study downward displacement flows along inclined pipes. We have recently studied in detail such displacement flows, in the iso-viscous Newtonian fluid setting^{6,7,8,9}, for viscosity ratios and shear-thinning fluids¹⁰, and for yield stress fluids¹¹. Each of these studies is targeted at pipe/duct inclinations close to horizontal.

Here we present results of a primarily experimental study of buoyant miscible displacement flows of a yield stress fluid by a higher density Newtonian fluid along a long inclined pipe. We focus on the industrially interesting case where the yield stress is significantly larger than a typical viscous stress in the displacing fluid, but where buoyancy forces may be significant.

EXPERIMENTAL SETUP

Our experimental study was performed in a 4m long, 19.05mm diameter, transparent pipe with a gate valve located 80cm from one end, see Fig. 1. The pipe was mounted on a frame which could be tilted to any angle. Initially, the lower part of the pipe is filled with a less dense fluid (fluid 2) coloured with a small amount of ink. The upper part of the pipe, above the gate valve, is filled by the denser fluid 1. To avoid pump disturbances, the displacing upper fluid was fed by an imposed over-pressure. The flow rate was controlled by a valve and measured by both a rotameter and

a magnetic flowmeter, located downstream of the pipe. At the start of the experiment the gate valve is opened. Images of the displacing fluid are recorded using 2 digital cameras, and subsequently analyzed to characterize different aspects of the flow. Velocity is also measured through the central plane of the pipe at a position downstream of the gate valve, using an Ultrasonic Doppler Velocimeter (UDV).

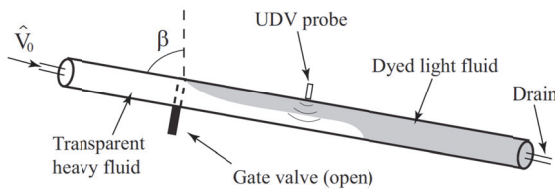


Figure 1. Schematic view of experimental set-up (the shape of the interface is illustrative only).

The displacing fluid 1 was always a Newtonian salt-water solution. Fluid 2 was always a yield stress fluid, namely a solution of Carbopol® EZ-2 polymer (Noveon Inc). Carbopol® is widely used as thickener, stabilizer and suspending agent. The rheology of Carbopol® is largely controlled by the concentration and pH of the solution. Once mixed with water, Carbopol® makes an acidic solution with no yield stress. The yield stress is developed at intermediate pH on neutralising with a base agent (in our case NaOH). The neutralised solution is fairly transparent and has the same density as water (for low concentrations).

PARMETER RANGE STUDIED

Our experiments covered a broad range of pipe inclinations and flow rates. The ratio between the yield stress and the viscous stress of the Newtonian displacing fluid is denoted by B_N , defined as:

$$B_N = \tau_Y D / \mu V_0 \quad (1)$$

and typically we have $B_N \gg 1$. Our flows are designed to be in laminar regime, when we consider the Newtonian fluid Reynolds number:

$$Re = \rho V_0 D / \mu \quad (2)$$

where $\rho = (\rho_1 + \rho_2)/2$. The other two most relevant dimensionless groups are

$$At = (\rho_1 - \rho_2) / (\rho_1 + \rho_2) \quad (3)$$

$$Fr = (At g D)^{1/2} \quad (4)$$

The ranges we have considered for our experiments are given in table 1.

Table 1. Parameter range for the experiments.

Parameter	range
β (deg)	0, 15, 30, 45, 60, 75, 83, 85
At	0.001, 0.0035, 0.01, 0.014, 0.016
V_0	0-120 mm/s
τ_Y	0-26 Pa
Re	0-2300
Fr	0.1-6
B_N	600-72000

RESULTS

We will describe our results in three main sections. Firstly, we describe our results for near horizontal pipe inclinations, as already reported¹¹. Thereafter we discuss differences that arise when the pipe is more inclined.

For near-horizontal pipes¹¹ we found that essentially two types of displacements occurred: central and slump displacements, as described below. These regimes were delineated exclusively by the value of Re/Fr , as shown in Fig. 2.

Central regime:

An example of a central-type displacement is given in Fig. 3a, showing a sequence of images as the displacing fluid advances through the pipe. The front shape is skewed towards the top of the pipe, which suggests inertial dominance at the tip/front. Purely viscous effects would lead to slumping. The bottom image shows the scale, which can be interpreted as a mean concentration at each position. We see darker regions at the top and bottom of the pipe, but also at mid-heights, all along the pipe. This is consistent with the presence of a residual wall layer all around the pipe. The images suggest that the layer is not uniform and further analysis reveals relatively long wavelength variations in layer thickness.

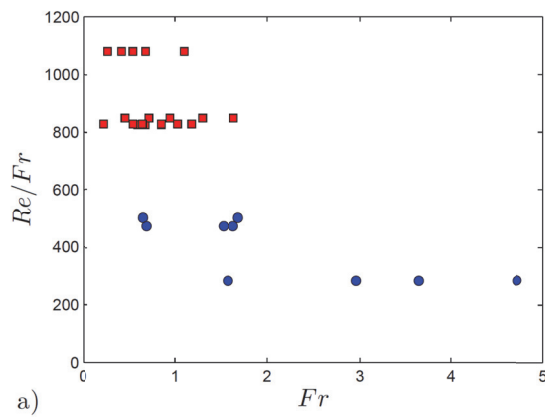


Figure 2. Classification of our results at inclinations for $\beta = 83^\circ$ & 85° , showing slump (squares) and central (circles) type displacements.

Fig. 3b shows measurements from the UDV probe. From the mean concentration we have inferred a mean residual wall layer thickness, and then calculated the axisymmetric flow two-layer flow corresponding to these parameters. The two-layer has a stationary wall layer and the velocity values correspond approximately to that from the UDV (although the measured velocity is slightly skewed).

Slump regime:

In a typical slump regime displacement the heavier displacing fluid advances in a layer (or layers) along the bottom of the pipe, possibly bypassing the stationary yield stress fluid above it. We show an example in Fig. 4a in which a single interface/layer advances along the pipe.

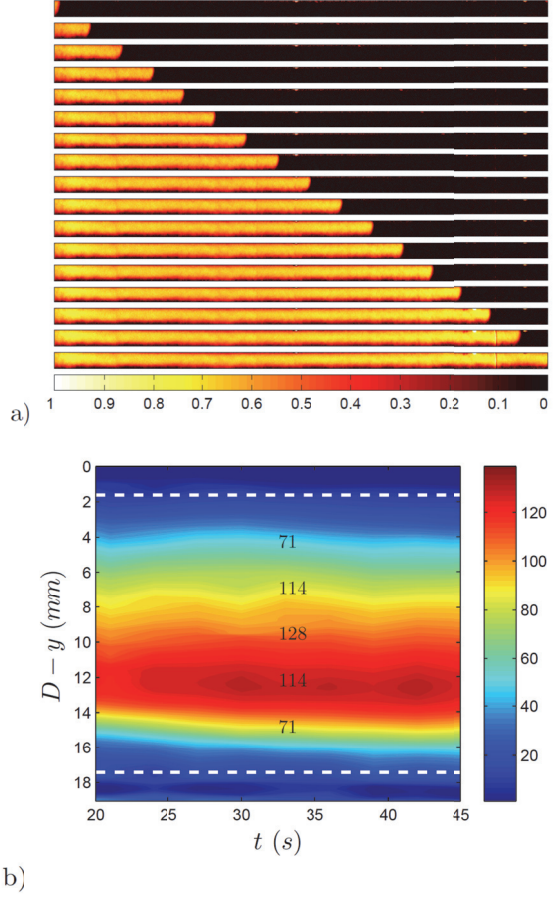
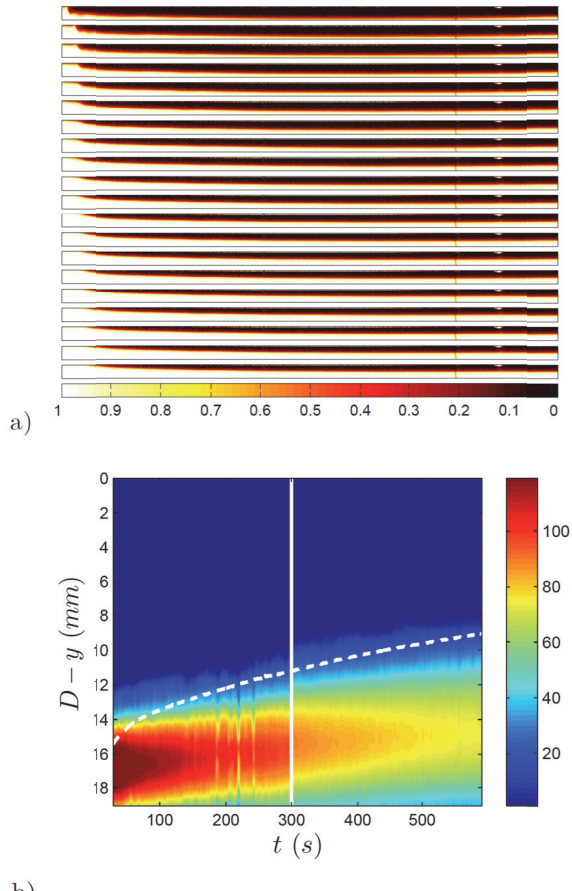


Figure 3. Central displacement for $\beta = 85^\circ$, $At = 4 \times 10^{-3}$ and $V_0 = 44\text{mm/s}$: a) images of the displacement at $t = 1, 2, \dots, 16, 17\text{s}$ after opening the gate valve. The length of pipe shown in a) is a 990mm long section, starting a few centimeters below the gate valve. b) Contours of velocity profiles obtained from the UDV at 80cm below the gate valve. Assuming a symmetric flow, velocity values from a simple two-layer Poiseuille profile surrounded by static layers are superimposed onto this plot. The broken lines show the position of the symmetric static layer, estimated from the mean concentration.

The UDV profile corresponding to Fig. 4a is shown in Fig. 4b, again with the interface height inferred from the measured concentration and superimposed as the broken white line on Fig. 4b. We can see from the measured velocity that the thick upper layer is largely static. As the displacement progresses the interface height increases and since the flow rate is fixed the velocity in the displacing fluid reduces.



b)

Figure 4. Slump displacement for $\beta=85^\circ$, $At=10^{-2}$ and $V_0=26\text{mm/s}$: a) a sequence of snapshots showing a 990 (mm) long section of the pipe a few centimeters below the gate valve at $t=30, 60, 570, 600\text{s}$ after opening the gate valve; b) contours of velocity from the UDV at 80cm below the gate valve.

The example shown in Fig. 4 is relatively simple, in comparison to some of the other slump type displacements observed¹¹. For

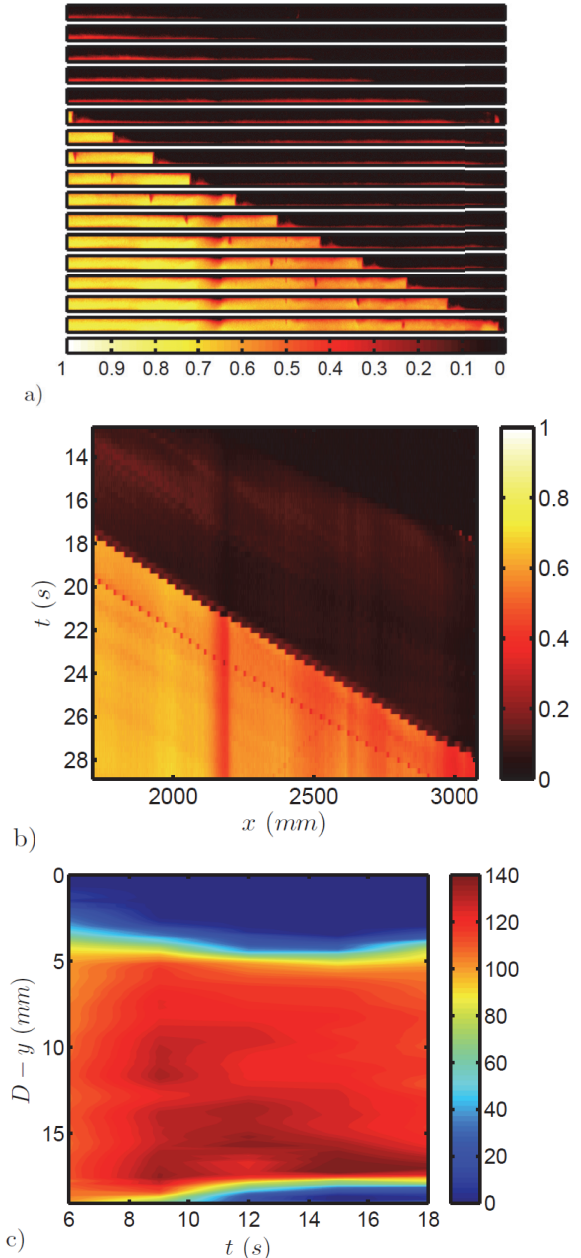


Figure 5. Slump-type displacement at $\beta=45^\circ$, $At=0.01$, $\tau_Y=7.9\text{Pa}$, $V_0=81.5\text{mm/s}$. a) Images of the displacement at $t=12, 13, \dots, 26, 27\text{s}$ after opening the gate valve. b) Spatiotemporal image of the same displacement. Note x is the streamwise distance measured from the gate valve. c) UDV plot of the same experiment (the UDV probe is located 156cm down the gate valve).

many displacements a thin front advances very rapidly along the bottom of the pipe, sometimes with unsteady ruptures of the gel above, believed to be related to transition to turbulence in the narrow channel.

Effects of inclination:

As pipe inclinations are reduced towards vertical, we continue to see both slump and central type displacements, but also observe other interesting behaviours.

Fig. 5 shows an example of a slump type displacement in which, as at high inclinations, an initially fast moving front advances, followed by a slower second trailing front.

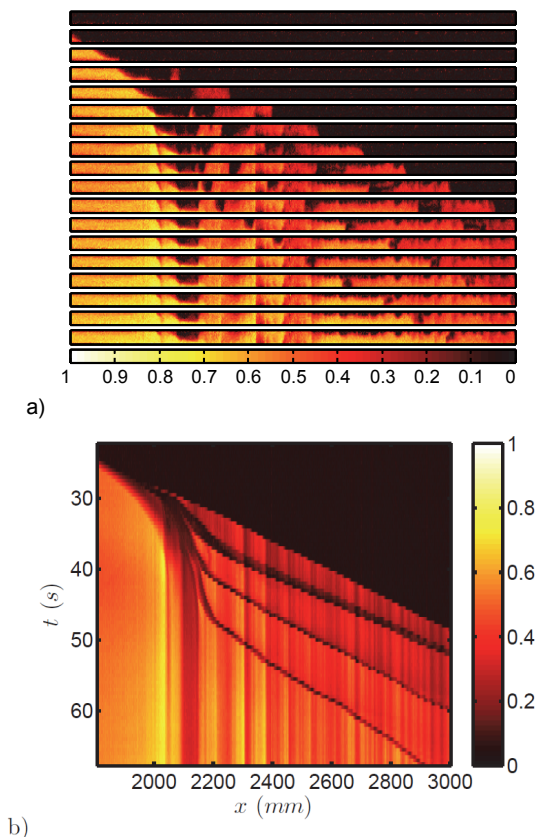


Figure 6. Slump-type displacement for $\beta=60^\circ$ At=0.016, $\tau_Y=14.9\text{Pa}$, $V_0 = 26.8 \text{ mm/s}$. a) Images of the displacement at $t = 22.5, 25, \dots, 62.5, 65\text{s}$ after opening the gate valve. b) Spatiotemporal image of the same displacement.

The UDV results (Fig. 5c) show that before the trailing front reaches the UDV position, the plug flow exists in the upper part of the pipe with a fast front moving beneath. After the trailing front passes by ($t \sim 9\text{s}$) there is static layer formed at upper and lower walls, and presumably all around the pipe walls. The thickness of the static layer is very small close to the lower wall. Also note that the velocity magnitudes within the displacing layer are larger as we get closer to the wall due to the existence of the fast front of displacing liquid¹¹.

A prevalent feature at inclinations away from horizontal is that the displacing fluid has a stronger axial buoyancy component and appears to by-pass the displaced fluid much more easily. Together with the unsteady flows common in slump-type displacements it is common to observe the development of slugging along the pipe, so that the yield stress fluid is displaced in a number of discontinuous stages. Examples are shown in Figs. 6 and 7, at slightly different inclinations and Atwood numbers.

Whereas for near-horizontal displacements unsteadiness was often caused by high speeds in a relatively narrow basal channel, here we may also begin to have interfacial type instabilities due to the increasingly strong axial buoyancy forces, which lead to regions of counter-current flow. Whatever the cause, we commonly observe pieces of yield stress fluid in the UDV graph (in this case at $t \sim 20$ and $t \sim 82\text{s}$) and are advected downstream by the mean flow.

Finally, at inclinations close to vertical and for stronger yield stresses, we see the development of interesting helical structures during the displacement; see Fig. 8. The UDV results clearly show a highly unsteady streamwise velocity component. This type of mode does occur in Rayleigh-Taylor type instabilities and it is not clear if this is the underlying instability mechanism here. Alternatively, one could view this as a

helical instability of a core-annular configuration.

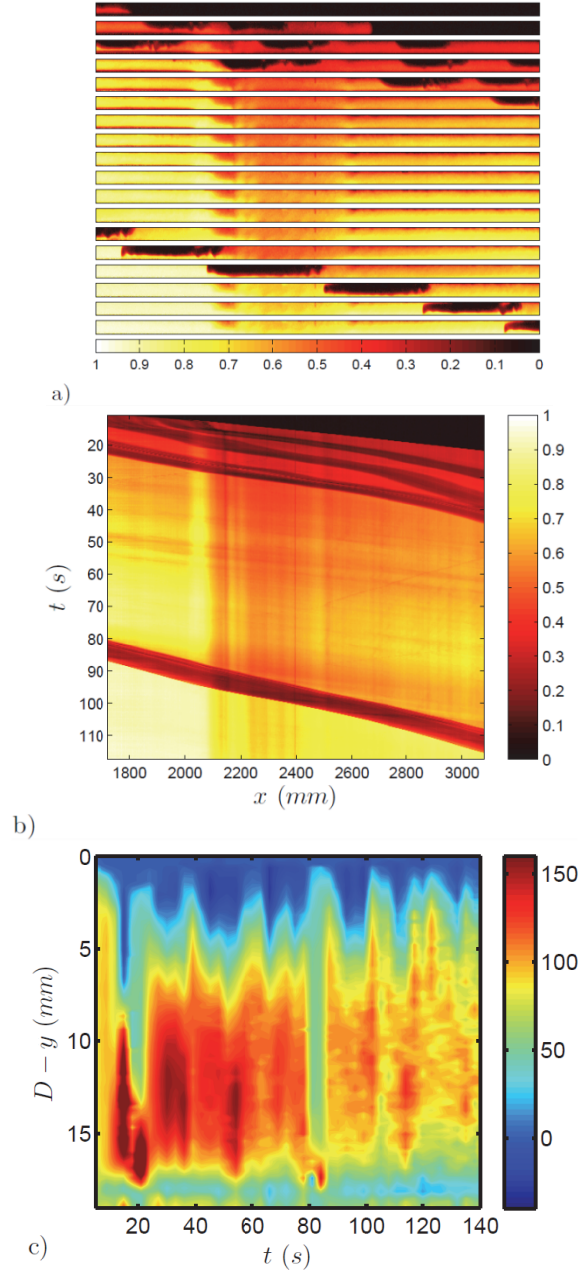


Figure 7. Slump-type displacement for $\beta = 45^\circ$ At=0.016, $\tau_Y = 16.4\text{Pa}$, $V_0 = 61.3\text{ mm/s}$. a) images of the displacement at $t = 22.5, 25, \dots, 62.5, 65\text{s}$ after opening the gate valve; b) Spatiotemporal image of the same displacement. c) UDV plot of the same experiment.

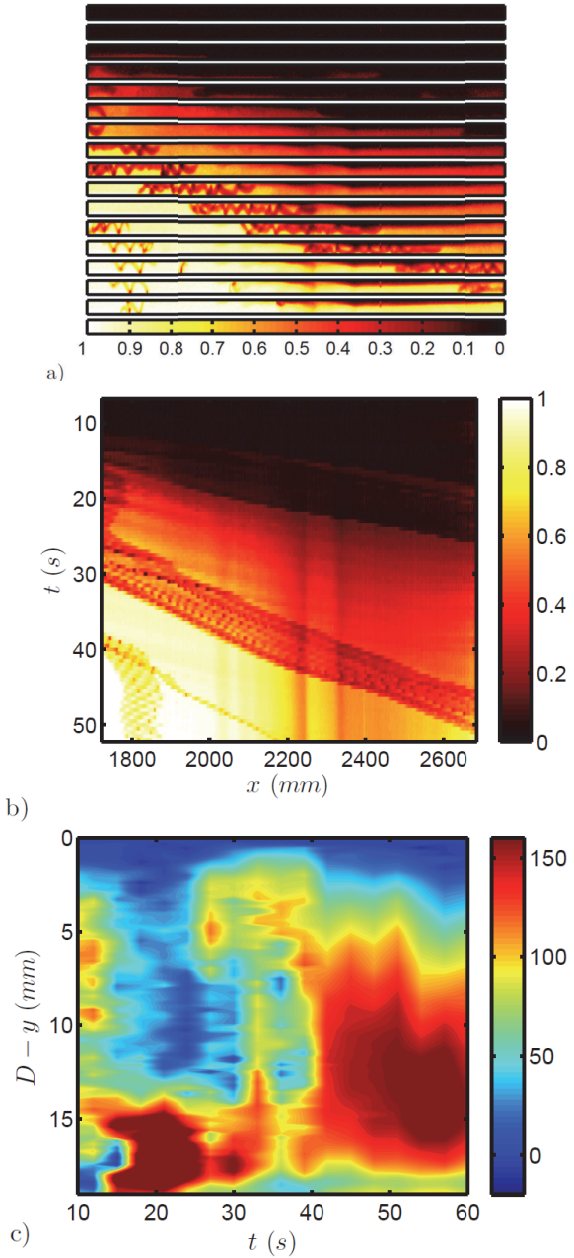


Figure 8. Helical instability for $\beta = 15^\circ$
At=0.016, $\tau_Y = 19.7\text{Pa}$, $V_0 = 61.3\text{ mm/s}$ a) images of the displacement at $t = 7, 10, \dots, 48, 52\text{s}$ after opening the gate valve; b) Spatiotemporal image of the same displacement. c) UDV plot of the same experiment.

In either case it is likely that at the large yield stresses in this experiment the stresses in the displacing fluid are insufficient to break up the helical column of yield stress fluid. For the experiment presented two

unstable pieces of yield stress fluid pass by the UDV location, at $t \sim 20$ s and $t \sim 33$ s respectively. This can be confirmed through the UDV results as well (see the enhanced jump in velocity around the given time).

At lower imposed flow rates, closer to an exchange flow regime, we have also observed helical backflows of the yield stress fluid, although here the yield stress fluid is displaced.

SUMMARY

We have presented experimental results in which a heavy Newtonian fluid displaces a lighter yield stress fluid in the downwards (density unstable) direction. We have focused on the industrially interesting case where the yield stress is significantly larger than a typical viscous stress in the displacing fluid, but where buoyancy forces may be significant.

A number of distinct flow regimes and exotic behaviours have been observed, due to the large yield stress of the displaced fluid. We have mostly presented the phenomenology of these flow regimes.

ACKNOWLEDGMENTS

This research has been carried out at the University of British Columbia, supported financially by NSERC and Schlumberger through CRD project 354716-07. The authors also thank Messrs Hady Abou Jaoude and George Hatzikiriakos for assisting in running the experiments.

REFERENCES

1. P.D. Howell, S.L. Waters, and J.B. Grotberg. *J. Fluid Mech.*, 406:309–335, 2000.
2. O. Wanner, H.J. Eberl, E. Morgenroth, D. Noguera, C. Picoreanu, B.E. Rittmann, & M.C.M. Van Loosdrecht. *IWA Scientific and Technical Report Series*, volume 18, pages 1–199. IWA Publishing, ISBN 1843390876., 2006.
3. G.K. Christian and P.J. Fryer. *Trans. IChemE C*, 84:320–328, 2006.
4. E.B. Nelson & D. Guillot. *Well Cementing, 2nd Edition*. Schlumberger Educational Services, 2006.
5. G. Vinay, PhD thesis, These de l’Ecole des Mines de Paris, Paris, France, 2005.
6. S.M. Taghavi, T. Seon, D.M. Martinez, and I.A. Frigaard. *J. Fluid. Mech.*, 639:1–35, 2009.
7. S.M. Taghavi, T. Seon, D.M. Martinez, and I.A. Frigaard. *Phys. Fluids*, 22:031702, 2010.
8. S.M. Taghavi, T. Seon, K.Wielage-Burchard, D.M. Martinez, & I.A. Frigaard. *Phys. Fluids*, 23:044105, 2011.
9. S.M. Taghavi, K. Alba, T. Seon, K.Wielage-Burchard, D.M. Martinez, & I.A. Frigaard. *J. Fluid Mech*, to appear in 2012.
10. S.M. Taghavi, K. Alba, and I.A. Frigaard. *Chem. Eng. Sci.*, 69:404–418, 2012.
11. S.M. Taghavi, K. Alba, M.A. Moyers-Gonzalez, & I.A. Frigaard. *J. Non-Newt. Fluid Mech.*, 167:59–74, 2012.